FRACTURE SPACING IN LAYERED MATERIALS: A NEW EXPLANATION BASED ON TWO-DIMENSIONAL FAILURE PROCESS MODELING

C. A. TANG*, Z. Z. LIANG*, Y. B. ZHANG*, X. CHANG*, X. TAO**, D. G. WANG**, J. X. ZHANG**, J. S. LIU***, W. C. ZHU***, and D. ELSWORTH[§]

ABSTRACT. Opening-mode fractures in layered materials, such as sedimentary rocks, pavement, functionally graded composite materials or surface coating films, often are periodically distributed with spacings scaled to the thickness of the fractured layer. The current general explanation is that when the fracture spacing to layer thickness ratio changes from greater than to less than critical values the normal stress acting perpendicular to the fractures changes from tensile to compressive. This stress state transition is believed to preclude further infilling of fractures, and the critical fracture spacing to layer thickness ratio at this point defines a lower limit, called fracture saturation. To better understand the controls on fracture spacing, we have investigated the problem using a progressive fracture modeling approach that shares many of the natural kinematic features, such as fracture nucleation, fracture infilling and fracture termination. As observed experimentally, our numerical simulations demonstrate that fracture spacing initially decreases as extensional strain increases in the direction perpendicular to the fractures, and at a certain ratio of fracture spacing to layer thickness, no new fractures nucleate (saturated). Beyond this point, the additional strain is accommodated by further opening of existing fractures: the spacing then simply scales with layer thickness, creating fracture saturation. An important observation from our fracture modeling is that saturation may also effectively be achieved by the interface delamination and throughgoing fracturing, which inhibit additional layer-confined fracturing. We believe that these processes may serve as another mechanism to accommodate additional strain for a fracture saturated layer. Because interface debonding stops the transition of stress from the neighboring layers to the embedded central layer, which may preclude further infilling of new fractures, our fracture modeling approach predicts a larger critical length scale of fracture spacing than that predicted by a stress analysis approach based on stress transition theory. Numerical simulations also show that the critical value of the fracture spacing to layer thickness ratio is strongly dependent on the mechanical disorder in the fractured layer. The spacing to thickness ratio decreases with increasing heterogeneity of the mechanical properties.

INTRODUCTION

Opening-mode fractures are common in both natural and manmade layered materials, including sedimentary rocks, pavement, functionally graded composite materials or surface coating films. They arise in materials which contract on cooling or drying, and are in many instances confined by layer boundaries with their height equal to the layer thickness (Helgeson and Aydin, 1991; Gross and Engelder, 1995; Fischer and others, 1995). This contraction, coupled with adhesion to neighboring layers, leads to a buildup of stress in the material, and when the stress exceeds the local tensile strength, fractures nucleate in the material. This relieves the stress locally along the sides of the fractures, but concentrates stress between the fractures. As a result, new fractures may infill between existing fractures and the fracture spacing decreases. The relation between fracture spacing and layer thickness has long been of interest in

*The State Key Laboratory of Coastal and Offshore Engineering, Dalian University of Technology, Dalian, China; catang@mechsoft.cn
**Center for Material Failure Modeling Research, Dalian University, Dalian, China
***School of Oil and Gas Engineering, the University of Western Australia, Crawley WA 6009, Australia
[§]Department of Energy and Geo-Environmental Engineering, Penn State University, University Park, Pennsylvania 16802

geosciences and material sciences, and has been studied by a number of investigators (Price, 1966; McQuillan, 1973; Narr and Lerche, 1984; Huang and Angelier, 1989; Narr and Suppe, 1991; Gross, 1993; Gross and others, 1995; Wu and Pollard, 1993, 1995; Becker and Gross, 1996; Ji and Saruwatari, 1998; Bai and Pollard, 2000a, 2000b; Bai and others, 2000). Commonly cited as a theoretical explanation for the linear relationship, Hobbs (1967) introduced for the first time the shear-lag model of Cox (1952), and modified the mathematical derivation of the model to incorporate an elastic layer-matrix system. In a more recent study (Ji and Saruwatari, 1998), the Hobbs model was revised to account for the non-linear decay of shear stress in the matrix.

The subject of fracture spacing was also investigated by field study (Gross, 1993) and experimental studies (Wu and Pollard, 1993, 1995). Wu and Pollard (1993, 1995) have demonstrated this process in four-point bending experiments with brittle coating materials. Their experiments showed that as the remote strain increases, the fracture spacing decreases approximately as the inverse of the remote strain, by fractures nucleating and propagating between earlier formed fractures. Eventually the fractures reach such a close spacing that no more fractures can infill, even with increasing strain. Instead, the existing fractures continue to open to accommodate the applied strain.

In the latest studies (Bai and Pollard, 2000a, 2000b; Bai and others, 2000), the spacing of fractures formed during the extension of layered rocks has been investigated using the finite element method. In these studies, the stress distribution between two adjacent fractures has been investigated as a function of the fracture spacing to layer thickness ratio using a three-layer elastic model with a fractured central layer. The results show that when the fracture spacing to layer thickness ratio exceeds a critical value, in the center between the fractures the normal stress acting perpendicular to the fractures changes from tensile to compressive. Bai and Pollard (2000a) concluded that this stress state transition precludes further infilling of new fractures unless either existing flaws are present or the fractures are driven by an internal fluid pressure.

Although the aforementioned explanation of fracture saturation has been widely accepted, few of the existing models can adequately reproduce the ongoing process of fracture nucleation, propagation, infilling and saturation, as observed experimentally. However, in our fracture modeling approach, we found that there are many other reasons that drive the system to reach the stage of fracture saturation. Two of the important reasons are the possible development of interface delamination and fractures passing through the layer boundaries. In addition, the analytical and numerical models considered so far tend to oversimplify the materials as a homogeneous medium. We note that failure phenomena depend very strongly on the properties of the material disorder and thus the involved materials cannot be treated as a homogeneous medium. Fracture of heterogeneous solids typically initiates from scattered weak sites in the medium which nucleate fractures upon exposure to a tensile stress. The nucleation of fractures is also heterogeneous in this case. The problem of how fractures in an embedded layer, particularly one with heterogeneous mechanical properties, initiate, grow and interact to produce the resulting fracture patterns remains largely unsolved. Therefore, a new theoretical understanding is needed.

The process of fracture formation in layered materials has been described as 'sequential infilling' (Hobbs, 1967; Gross, 1993), and the point where no more fractures can infill is called fracture saturation (Wu and Pollard, 1995; Bai and Pollard, 2000a). Similar terms were proposed in other literature (Garrett and Bailey, 1977a, 1977b; Parvizi and Bailey, 1978; Cobbold, 1979; Narr and Suppe, 1991; Wu and Pollard, 1991; Rives and others, 1992). To better understand the mechanisms of sequential infilling and to explain fracture saturation, we present new numerical modeling results, which are the focus of this paper. Of interest are the ensuing pattern of fractures and the dependence of the fracture spacing on the strain. We consider

three-layer material models with an embedded layer that fractures under a quasistatical, slowly increasing strain (induced, for example, by temperature changes, by desiccation, or by mechanical deformations); this situation is of common occurrence, see Bai and others (2000) for a general survey. In most of the stress analysis approaches, the fractures have to be inserted in the model, and the fracture forming process cannot be modeled. In this paper we describe a series of numerical simulations, using a RFPA (Realistic Fracture Process Analysis) code in which the progressive evolution of a fracture set is modeled during a controlled loading sequence, thus providing direct observations of the different stages in the development of the fracture set, from initiation to saturation. Unlike static stress analysis approaches in which the fractures have to be inserted in the model (Bai and others, 2000), our numerical code can model the complete fracture forming process. This fracture modeling technique can provide valuable insight concerning fracture processes that are impossible to observe in nature and difficult to consider using static stress analysis approaches. By changing the layer thickness and the material heterogeneity of the model we are able to examine how spacing is dependent upon thickness and heterogeneity at each stage of development. For simplicity, we postulate that the mechanical central layer has a lower strength so that the fracture nucleation is confined in this single layer.

We first validate the model by comparing the stress states between two adjacent fractures for a typical three-layer model with available data from literature (for example, Bai and Pollard, 2000a, 2000b; Bai and others, 2000). We then apply the same three-layer model, but without pre-existing fractures, to investigate the progressive evolution of fracture populations in space, as a function of the applied strain. Material heterogeneity of the mechanical properties is considered in our modeling studies. The models are loaded by mechanical stretch in a displacement-controlled manner, and the process of fracture infilling and saturation is the consequence of the mechanical loading. We check the fracture spacing as a function of the average applied strain, the fracture spacing to layer thickness ratio, and the influence of heterogeneity of the material properties on this ratio. Finally, the implications of the results for the study of fracture spacing in layered rock are discussed.

In this paper, based on the definition by Bai and others (2000), the term "fracture" is used to represent any fracture that cuts or almost cuts through the fractured layer. The term "flaw" is used for a crack that is very short compared to the thickness of the fractured layer. Fractures form by propagation of flaws or coalescence of multi-flaws.

NUMERICAL METHOD AND VERIFICATION

Numerical Method

We use a two-dimensional finite element code named RFPA^{2D} (Realistic Failure Process Analysis code). This code is based on the theory of elastic-damage mechanics, and was originally developed by Tang (1997), based on FEM (finite element method) and improved at Mechsoft, China (RFPA User Manual, 2005). The code and the user manual can be freely downloaded from www.rfpa.cn.

In RFPA^{2D}, the solid or material is assumed to be composed of many elements with the same size, and the mechanical properties of these elements are assumed to conform to a given Weibull distribution as defined in the following function:

$$f(u) = \frac{m}{u_0}\left(\frac{u}{u_0}\right)^{m-1}\exp\left[-\left(\frac{u}{u_0}\right)^m\right] \qquad (1)$$

where u is the parameter of the element (such as strength or elastic modulus); the scale parameter, u_0, is related to the average of the element parameter and the shape

parameter, *m,* defines the shape of the distribution function. According to the definition, a larger *m* implies a more homogeneous material. We therefore call this parameter (m) the homogeneity index. In general, we assumed that the Young's modulus and strength (compression and tension) of mesoscopic elements that are used to simulate a rock specimen conform to two individual distributions with the same homogeneity index. The mesoscopic elements are assumed to be isotropic and homogeneous.

At the beginning, the element is considered elastic, and its elastic properties can be defined by Young's modulus and Poisson's ratio. The stress-strain curve of an element is considered linear elastic until the given damage threshold is attained, and then is followed by softening. We choose the maximum tensile stress criterion and Mohr-Coulomb criterion respectively as the damage thresholds (Brady and Brown, 1993; Tang, 1997).

In elastic damage mechanics, the elastic modulus of the element may degrade gradually as damage progresses. The elastic modulus of damaged material is defined as follows (Tang, 1997).

$$E = (1 - \omega)E_0 \tag{2}$$

where ω represents the damage variable, E and E_0 are elastic moduli of the damaged and the undamaged material, respectively. Here the element as well as its damage is assumed isotropic and elastic, so the E, E_0 and ω are all scalar.

When the mesoscopic element is under a uniaxial stress state (including uniaxial compression and uniaxial tension), the constitutive relationship of elements is shown in figure 1. At the beginning, the stress-strain curve is linear elastic and no damage occurs, that is $\omega = 0$. When the maximum tensile strain criterion is met, the damage of the element occurs.

The constitutive relationship of a microscopic element under uniaxial tension as shown in the third quadrant of figure 1 can be expressed as

$$\omega = \begin{cases} 0 & \varepsilon > \varepsilon_{t0} \\ 1 - \dfrac{f_{tr}}{E_0\varepsilon} & \varepsilon_{tr} < \varepsilon \leq \varepsilon_{t0} \\ 1 & \varepsilon \leq \varepsilon_{tu} \end{cases} \tag{3}$$

where f_{tr} is the residual tensile strength defined as $f_{tr} = \lambda f_{t0} = \lambda E_0\varepsilon_{t0}$; f_{t0} and λ are uniaxial tensile strength and residual strength coefficients, respectively; ε_{t0} is the strain at the elastic limit (also called threshold strain); and ε_{tu} is the ultimate tensile strain of the element, at which the element would be completely damaged. The ultimate tensile strain is defined as $\varepsilon_{tu} = \eta\varepsilon_{t0}$, where η is called ultimate strain coefficient. Equation (3) can be expressed as

$$\omega = \begin{cases} 0 & \varepsilon > \varepsilon_{t0} \\ 1 - \dfrac{\lambda\varepsilon_{t0}}{\varepsilon} & \varepsilon_{tu} < \varepsilon \leq \varepsilon_{t0} \\ 1 & \varepsilon \leq \varepsilon_{tu} \end{cases} \tag{4}$$

Additionally, we assume that the damage of a mesoscopic element in a multiaxial stress condition is also isotropic and elastic. According to the method of extending a one-dimensional constitutive law under uniaxial tension to a complex stress condition, we can easily extend the constitutive law described above to use for three-dimensional stress states when the tensile strain threshold is attained. Under multi-axial stress states the element still damages in tensile mode when the equivalent major tensile strain $\bar{\varepsilon}$
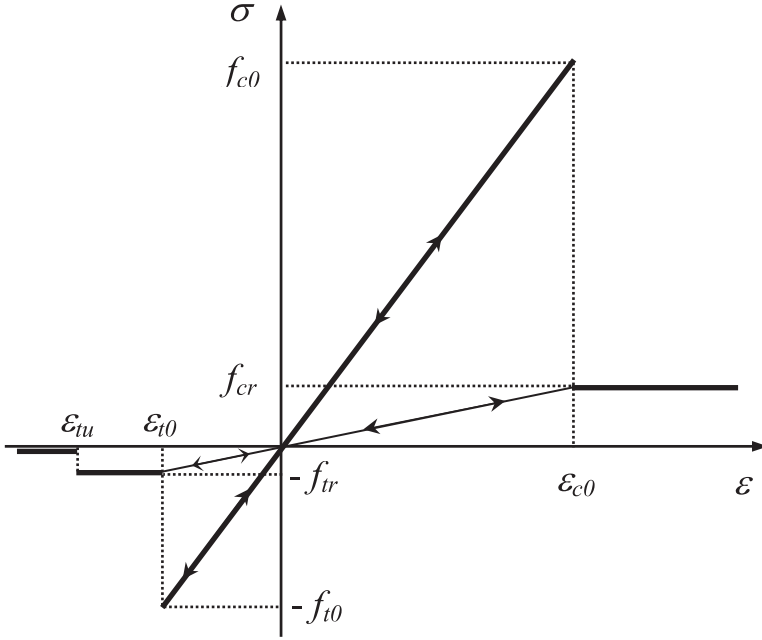
Fig. 1. Elastic damage constitutive law of elements under a uniaxial stress state where f_{t0} and f_{tr} are uniaxial tensile strength and residual uniaxial tensile strength of element, respectively; and f_{c0} and f_{cr} are uniaxial compressive strength and corresponding residual strength of element, respectively.

attains the above threshold strain ε_{t0}. The equivalent principal strain $\bar{\varepsilon}_{t0}$ is defined as follows:

$$\bar{\varepsilon} = - \sqrt{\langle -\varepsilon_1 \rangle^2 + \langle -\varepsilon_2 \rangle^2 + \langle -\varepsilon_3 \rangle^2} \tag{5}$$

where ε_1, ε_2 and ε_3 are three principal strains, and $\langle\ \rangle$ is a function defined as follows:

$$\langle x \rangle = \begin{cases} x & x \geq 0 \\ 0 & x < 0 \end{cases} \tag{6}$$

The constitutive law of the element subjected to multiaxial stresses can be easily obtained only by substituting the strain, ε, in equations (3) and (4) with the equivalent strain, $\bar{\varepsilon}$. The damage variable is expressed as

$$\omega = \begin{cases} 0 & \bar{\varepsilon} > \varepsilon_{t0} \\ 1 - \dfrac{\lambda \varepsilon_{t0}}{\bar{\varepsilon}} & \varepsilon_{tu} < \bar{\varepsilon} \leq \varepsilon_{t0} \\ 1 & \bar{\varepsilon} \leq \varepsilon_{tu} \end{cases} \tag{7}$$

In order to study the damage of an element when it is under compressive and shear stress, the Mohr-Coulomb criterion is chosen to be the second damage threshold.

$$F = \sigma_1 = \frac{1 + \sin \varphi}{1 - \sin \varphi} \sigma_3 \geq f_{c0} \tag{8}$$

where σ_1 and σ_3 are major and minor principal stress respectively; f_{c0} is the uniaxial compressive strength and φ is the internal friction angle of the mesoscopic element. Again, compressive stresses are positive and tensile stresses are negative. As a matter of fact, the numerical values of σ_1 and σ_3 indicate the magnitude of maximum and minimum compressive stresses, respectively, when these two principal stresses are both compressive. In the same way, when the element is under uniaxial compression and damaged according to the Mohr-Coulomb criterion, the similar expression for the damage variable, ω, can be described as follows:

$$\omega = \begin{cases} 0 & \varepsilon < \varepsilon_{c0} \\ 1 - \dfrac{\lambda \varepsilon_{c0}}{\varepsilon} & \varepsilon \geq \varepsilon_{c0} \end{cases} \tag{9}$$

where λ is the residual strength coefficient. We assumed that $f_{cr}/f_{c0}=f_{tr}/f_{t0}=\lambda$ is true when element is under uniaxial compression or tension.

When an element is under a multi-axial stress state and its strength satisfies the Mohr-Coulomb criterion, damage occurs, and we must consider the effect of other principal stresses in this model during the damage evolution process. When the Mohr-Coulomb criterion is met, we can calculate the maximum principal strain (maximum compressive principal strain)ε_{c0} at the peak value of maximum principal stress (maximum compressive principal stress).

$$\varepsilon_{c0} = \frac{1}{E_0} \left[f_{c0} + \frac{1 + \sin \varphi}{1 - \sin \varphi} \sigma_3 - \mu(\sigma_1 + \sigma_2) \right] \tag{10}$$

In this respect, we assume that the shear damage evolution is only related to the maximum compressive principal strain, ε_1. So, we use the maximum compressive principal strain, ε_1, of the damaged element to substitute the uniaxial compressive strain, ε_{c0} in equation (9). Thus, the former equation (9) can be extended to triaxial stress states for shear damage.

$$\omega = \begin{bmatrix} 0 & \varepsilon_1 < \varepsilon_{c0} \\ 1 - \dfrac{\lambda \varepsilon_{c0}}{\varepsilon_1} & \varepsilon_1 \geq \varepsilon_{c0} \end{bmatrix} \tag{11}$$

In summary, our numerical approach to the fracture problem can be described as the following: The embedded layer is brittle, so that each element can fail under stress. Our numerical simulation involves the calculation of the stresses acting on the elements and the mechanical property change of the damaged elements according to the constitutive laws and strength criterion described above. The value at which a particular element fails is random, but fixed at the start of the modeling process (that is, the disorder is quenched). The statistical distribution of the breakdown thresholds is a material property and is described by equation (1). Under a quasi-statically increasing external stretch the stress or strain of the elements are given by the solution of the FEM for mechanical equilibrium at each FEM node. If the stress of an element attains its prescribed breakdown strength, the element fails irreversibly, and its elastic constant is changed according to its post-failure law, as described above. This is followed by additional relaxation steps, in which the new equilibrium positions are calculated. In the brittle regime these steps may lead to the failure of additional elements. Iterating the procedure leads to fracture propagation, where fractures are defined by groups and alignments of failed elements.

Our method is similar to the one that Spyropoulos and others (2002) used in their study of the problem of the crack population formation and its evolution on a brittle
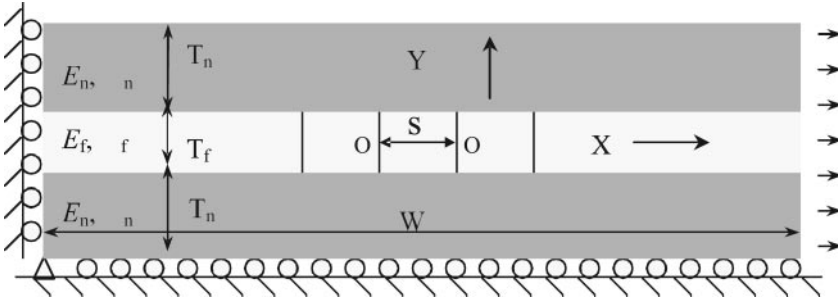
Fig. 2. The three-layer model and its boundary conditions. The X direction is parallel to the layer boundaries and perpendicular to the fractures. The Y direction is perpendicular to the layer boundaries. The thickness of central layer and neighboring layers are indicated with T_f and T_n, respectively. The spacing between adjacent fractures is denoted as S, and the model width is defined as W.

layer that is driven on the bottom by an extending layer. In their model, the lower plastic layer is extended by a small amount. That in turn strains the top layer whose equilibrium requirement is satisfied when the total stresses applied to it are lower than its yield strength. If at any point on the brittle layer the yield strength is exceeded, a crack is allowed to form. The crack accumulates slip until the stress on it satisfies the boundary condition, and the system has reached quasistatic equilibrium. It gets driven by additional extension applied to the bottom layer, and the process repeats itself.

Verification of the Numerical Method

Before reporting the results of our simulations in progressive fracture modelings we first focus on verifying the model by carrying out analysis of stress that governs the model's behaviour. To do this we will consider a model put forth by Bai and others (2000). In the same way as Bai and others (2002), we investigate the stress state transition between adjacent equally spaced fractures. The model, its boundary and loading conditions, and the FEM mesh are shown in figure 2. The mesh was refined by reducing the sizes of the elements until calculated stresses differed by less than 0.1 percent in the central layer. The fractured central layer has a thickness $T_f =$30mm, which is also the height of the fractures (H). The overall thickness of the model ($T = T_f + 2T_n$) is 120mm. The model has a width $W=$400mm and contains a total of 48,000 elements, each 1 mm square. For this layered model, we postulate the two materials across the layer boundaries are welded together, that is no slip is permitted along the layer boundaries, and we postulate a plane strain condition for the entire model. The Young's moduli and Poisson's ratios for the adjacent layers are listed in table 1.

We fix the whole bottom boundary of the model in the *y*-direction, the whole left boundary of the model in the *x*-direction, and the left corner of the model in both *x* and *y*-directions as well. Loading is applied through imposed uniform lateral displacements prescribed over right vertical face with the opposite face fully restrained. The top boundary is free to displace as necessary to produce the designed values of average strain in the x-direction for the study of the average strain effect on the critical spacing to layer thickness ratio. Vertical displacements are unrestrained on the vertical model sides. Mean horizontal strain is applied to a maximum of 0.075 percent.

In the following validation analysis, four fractures are pre-assigned in the central layer. They are equally-spaced along the central layer, perpendicular to the long axis, and fully transect the layer height (300 mm) with an aperture of 0.1 mm. The two central fractures are used to represent any two adjacent fractures in a row composed of many members, as only the two end segments will have different stress distributions

TABLE 1

Young's moduli and Poisson's ratios for adjacent layers

Refer to	Layer level	E (GPa)	v	σ_c (MPa)	σ_t (MPa)	m	Layer size	Number of elements
Fig.2	Central layer	50	0.25	-	-	100	30mm×400mm	12000
	Top and bottom layer	10	0.35	-	-	100	45mm×400mm	18000
Fig.6	Central layer	50	0.25	-	-	2	30mm×400mm	12000
	Top and bottom layer	10	0.35	-	-	6	45mm×400mm	18000
Fig.8	Central layer	50	0.25	100	10	2	30mm×400mm	12000
	Top and bottom layer	10	0.35	200	20	6	45mm×400mm	18000
Fig.11	Central layer	50	0.25	100	10	2		
	Top and bottom layer	10	0.35	200	20	6		
Fig.13	Central layer	50	0.25	100	10		30mm×600mm	18000
	Top and bottom layer	10	0.35	200	20		45mm×600mm	27000

from the other segments (Bai and Pollard, 2000). With this defined geometry, the evolution of the stress distribution is examined as a function of the fracture spacing to the fractured layer thickness ratio.

To develop a clear understanding of the transition in horizontal stress (σ_x) along line O-O of figure 2 for a homogeneous medium, the homogeneity index is set to represent a uniform material with m large enough to represent a very homogeneous material. As shown in figure 3, the critical fracture spacing to fracture layer thickness ratio is about 1.0 (normal stress is zero in the central area between the adjacent fractures). This critical value determines the stress state between the adjacent fractures: when the ratio is below this critical value the stress along the segment O-O is compressive, and while above this critical value the stress is tensile. This is confirmed by the results of the stress distribution in figure 3. As illustrated in figure 4, the periodic distribution of stresses between fractures is shown to change as the fracture spacing to layer thickness ratio (S/T_f) transits the threshold of unity.

As shown in figure 3, the stress along line O-O reaches a peak value at the mid-point between adjacent fractures. This stress state varies with the S/T_f ratio, as shown in figure 5. Our results agree well with the numerical results obtained by Bai and Pollard (2000a). Bai and Pollard (2000a) recognized that the stress state between the adjacent fractures is determined by three mechanisms. The first mechanism is the transfer of stress from adjacent layers, which can only produce tensile stress (σ_{Txx}) in the central area. The second mechanism involves the contraction of the fractured layer in the vertical direction as the fractures shorten and correspondingly open. The central layer contracts more when fractures are present than when they are absent, and when longitudinal extension is applied, which can produce a vertical compressive stress. Because of the constraint in the horizontal direction, the vertical compressive stress can produce a horizontal stress (σ_{Cxx}). The third mechanism is the effect of the traction-free fracture surface, which eliminates both the transferred stress and the effect of horizontal constraint near the fractures. The horizontal stress (σ_x) between two fractures is determined by the relative magnitudes of the transfer stress and the compressive stress mentioned above, which can be described as $\sigma_x = \sigma_{Cxx} + \sigma_{Txx}$. The results from our model runs support these observations.
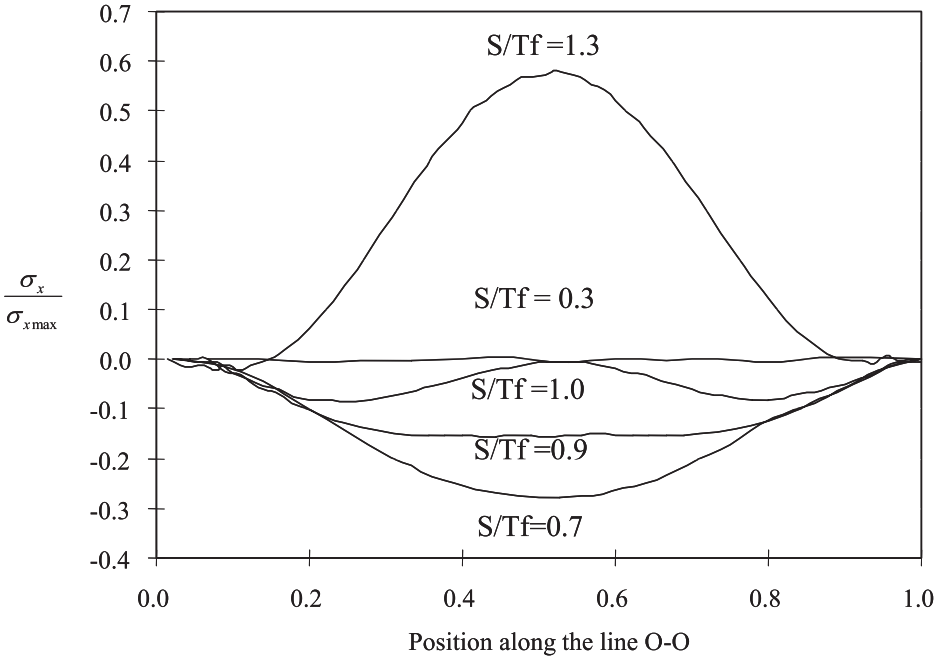
Fig. 3. The distribution of σ_x along the line O-O with different fracture spacing to thickness ratios (S/T_f), where the positive sign represents tensile stress and the negative sign represents compressive stress.

As real materials, especially rocks, are never homogeneous because they contain inhomogeneities and defects at various length-scales, it is necessary to consider this local-scale heterogeneity in fracture modeling. In our numerical study, this is accommodated by the implicit inclusion of heterogeneity through the Weibull parameter, *m,* as described in equation (1). The FEM model we used comprises a large number of elements, and its local heterogeneity is determined by assigning to each element a group of mechanical parameters, such as Young's modulus, strength, *et cetera*, from the given statistical distribution [equation (1)]. The extent of the heterogeneity is represented by an index of *m*.

The situation for heterogeneous models is considerably more complex than in homogeneous models. Here a different and very important feature appears, namely, small scale stress fluctuation. We use a model with the same geometry as in figure 2, but with heterogeneity considered in the model (*m*=2), as shown in figure 6. The other parameters are the same as those used in figure 2 (see table 1 for fig. 6).

In figure 7, as in figure 3, we display the stress (σ_x) along the section O-O indicated in figure 6. Stresses are shown to fluctuate around the mean stress of the homogenous material, but give a local variation that is conditioned by the magnitude of mean stress. Expected from this is that local fluctuations in stress and in strength will create local conditions where fractures are more likely to nucleate and grow, which, in turn, may correspondingly affect the resulting fracture patterns. Consequently, a smaller critical length scale of fracture spacing comparing with the homogeneous model is expected. The following numerical results regarding fracture pattern for heterogeneous materials show that during the process of fracture infilling the new fracture does not always initiate at the middle point between the earlier formed fractures. Instead, the new fracture initiates at a point where the local element stress reaches its failure strength.

$$\frac{S}{T_f} = 1.3$$

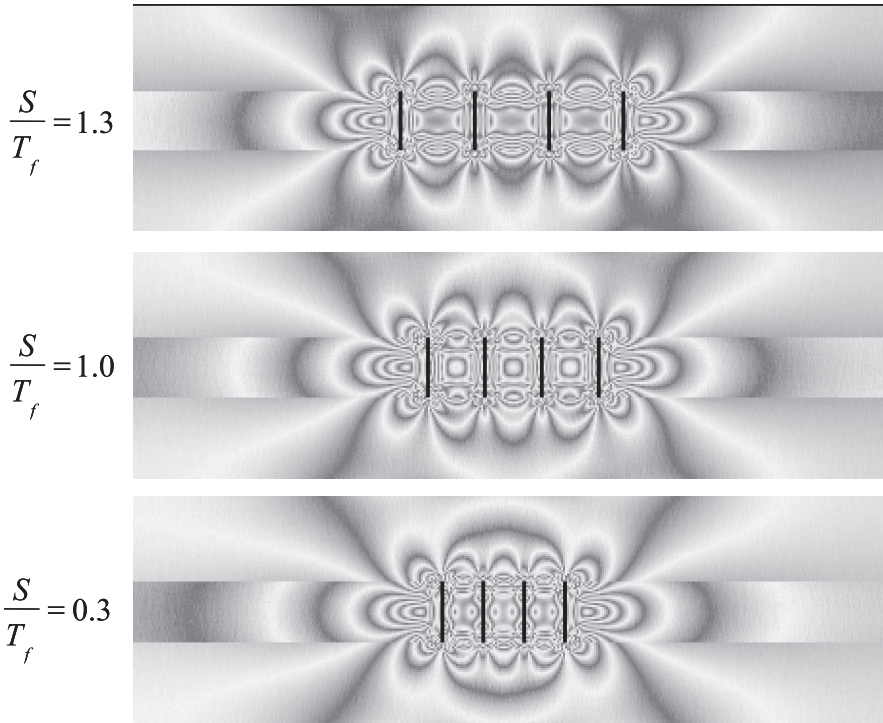$$\frac{S}{T_f} = 1.0$$

$$\frac{S}{T_f} = 0.3$$

Fig. 4. Modeled fringe contours in layers under different fracture spacing to thickness ratio. (Note: One of the most widely used techniques to visualize stress fields is the technique of photoelasticity. Photoelasticity provides the contours of difference in principal stresses. The contours are generally observed as fringes, and fringes are usually numbered as 0, 1, 2, 3,. . . *et cetera*, depending on the specific optical arrangements employed. The fringes in general appear as broad bands, the thickness of the fringe is indicative of the gradient of the stress variable. The fringes are very broad when the gradient is small, and *vice versa*. Further, a zone of high density of fringes indicates a zone of stress concentration. Thus, a mere qualitative observation of the fringes can yield a wealth of useful information about stress distribution)

The above analysis of stress between the pre-existing fractures shows that, as fractures behave as free surfaces, as a result, the normal stress in the vicinity of a fracture is greatly reduced, thereby inhibiting the formation of new fractures. This zone of reduced stress, referred to as the stress reduction shadow (Becker and Gross, 1996), scales with fracture height and is considered to be responsible for the observed correlation between fracture spacing and layer thickness (Cox, 1952; Lachenbruch, 1961; Hobbs, 1967; Pollard and Segall, 1987).

MODELING OF FRACTURE PROCESSES IN A THREE LAYER MODEL

In the previous section, we confirm that there is a stress state transition between two adjacent opening-mode fractures in a layered model under extension. In this section, the numerical code described above is applied to model the fracture pattern of the same three-layer model, but without pre-existing fractures. The models are loaded by mechanical stretch in a displacement controlled manner, and the process of progressive fracture infilling and saturation is the consequence of the mechanical loading. This fracture modeling provides us with a unique opportunity to investigate the mechanism of how a fracture set evolves with increasing applied strain, thereby factoring out the effects of layer thickness and mechanical properties.
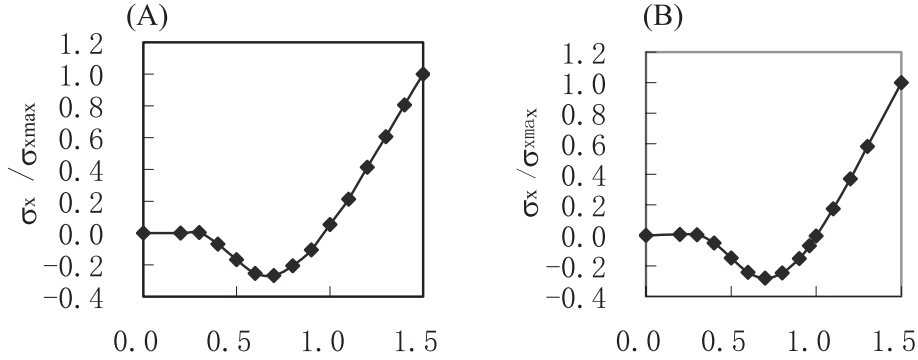
Fig. 5. The transition of stress σ_x at the middle point of the line O-O relative to fracture spacing to thickness ratios (S/T_f). Tensile stresses are positive, and compressive stresses are negative. The material is homogeneous. (A) Obtained from RFPA^{2D}, (B) Results of Bai and Pollard (2000) for the same problem.

Fracture Infilling and Fracture Saturation

Table 1 (for fig. 8) also lists the mechanical properties and the model and mesh characteristics adopted for this analysis. Strains are applied to the model through the application of lateral displacements to the model ends. The total strain is applied in 240 increments, from an initial value of 0 to a final value of 0.048 percent.

Figure 8 illustrates the numerically obtained fracture infilling process and fracture saturation. According to the order of the fracture formation, we can divide the whole process into four stages. In the first stage (figs. 8A and 8B), before strain reaches 0.086×10^{-3}, randomly distributed short fractures form in the central layer at its weak locations, where the local tensile stress reaches the local tensile strength. During this stage, the tensile stress results mainly from the tensile strain applied to the model ends. The initial fractures are isolated from these seed locations and do not interact. In the second stage (figs. 8B and 8D), four long fractures form sequentially. In the third stage (figs. 8E–8J), six additional fractures nucleate and infill between these first four fractures. Finally, upon reaching the ultimate strength of the neighboring layers, catastrophic failure occurs when a large, opening mode fracture propagates across the entire model. This throughgoing fracture precludes further fracture infilling, so that even large increments of strain did not result in the formation of additional infilling fractures (figs. 8K and 8L). Prior to throughgoing fracture, all the fractures are mechanically confined, and arrest at layer boundaries during sequential infilling.

Figure 9 shows the temporal distribution of fracture events that occurred during the loading process. The curve correlates the fracture event counts with the fracture infilling phenomenon very well. It is seen from figure 9 that in the less advanced stage I, a steadily increasing number of small fractures occur, because lower strength flaws propagate earlier due to their lower critical fracture stresses. However, during the stages II and III, the number of flaw nucleation events no longer increases systematically with increasing strain. Rather, the progressive development of fracture events with increasing strain is characterized by a shift from a broad distribution to a narrow distribution. The dramatic decrease in local tensile stress between adjacent fractures and the increase in critical fracture stress cause additional fracturing to occur only after an incremental threshold strain. In other words, once a thickness cut-through fracture nucleated, the layer generally remains stable during gradual increases in extensional strain up until the point where critical stress is achieved between adjacent fractures. As shown in figure 9, whereas the magnitude of extensional strain increases gradually within the layer, changes in fracture spacing are abrupt. A comparison
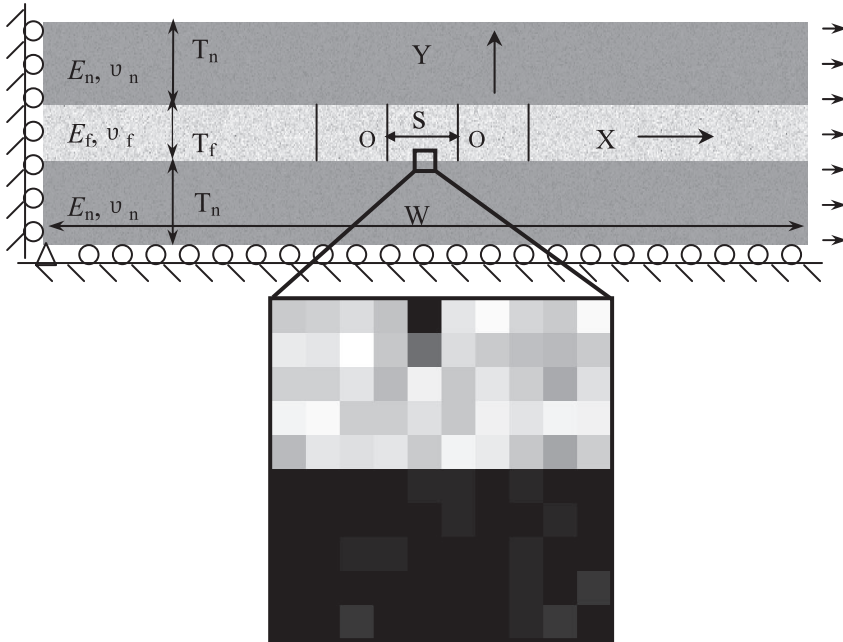
Fig. 6. The three-layer model and its boundary conditions with heterogeneity of mechanical properties considered. The X direction is parallel to the layer boundaries and perpendicular to the fractures. The Y direction is perpendicular to the layer boundaries. The thickness of central layer and neighboring layers are indicated with T_f and T_n, respectively. The spacing between adjacent fractures is denoted as S, and the model width is defined as W. The box shows in detail the heterogeneity in the model. As the model has 48000 elements and the scale of the elements is too small to identify the element mesh, we show a small portion of the model in a big box. The different gray color in the box represents different value of mechanical properties of the individual element.

between figure 8 and figure 9 reveals that each abrupt increase in fracture event counts corresponds to an event of fracture infilling. For the throughgoing fracture that occurred in the final stage, the curve shows a sudden stress drop to zero and an abrupt increase of fracture event counts.

Figure 10 shows the numerically obtained relationship between the fracture spacing to layer thickness ratio and strain. It is shown that this ratio decreases with increasing strain.

Critical Ratio of Fracture Spacing to Layer Thickness

In order to study the dependence of critical fracture spacing on the layer thickness, five models with different values of layer thickness (T_f = 15, 20, 25, 30 and 35mm) are used. We select $T_n = 2T_f$. All the other mechanical properties are shown in table 1 for figure 11. Strains are applied to the model through the application of lateral displacements to the model ends. The total strain is applied in 110 increments, from an initial value of 0 to a final value of 0.022 percent.

Figure 11 shows the three layer models and the numerically obtained fracture spacing at saturation. All of the simulations produce a similar relationship between spacing and thickness: spacing decreases rapidly with strain in the early stages of the simulation and then decreases less rapidly, finally reaching a nearly constant value. In other words, great applied strain beyond some limiting value will not change the spacing significantly. This is the so-called "fracture saturation" (Wu and Pollard, 1991,
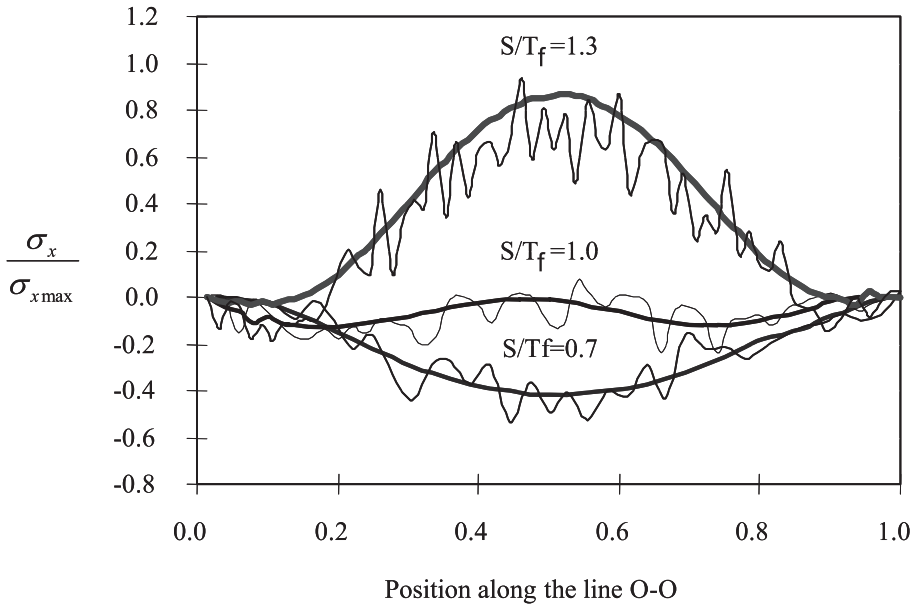
Fig. 7. The distribution of σ_x along the line O-O shown in figure 2 with different fracture spacing to layer thickness ratios (S/T_f). The homogeneity indices are $m=2$ for the thick lines representing relatively heterogeneous material, and $m=1000$ for the thin lines representing relatively homogeneous material, respectively. Positive stresses are tensile.

1992). Comparing the two extreme thicknesses from our numerical simulations, T_f =15mm and T_f =35mm, critical ratio for saturation spacing increases systematically from 1.67 to 2.28 under the same applied strain.

By plotting the critical fracture spacing to layer thickness ratio (S/T_f at fracture saturation) versus layer thickness (T_f), we obtain the relation shown in figure 12. Each point on this graph represents the mean value of four simulations of spacing S at the critical strain. Although there is scatter in the data on spacing, the slope of the curve in this figure is found clearly to be positive. That is, the critical fracture spacing to layer thickness is linearly related to the layer thickness. We did more than 20 runs with the same models and found that this is not a result of mesh effect problem. We then believe that this is a size scale dependent problem. It is important to mention that when we studied this relationship with the same models based on a stress analysis approach (that is, only calculate the stress distribution without fracture modeling), we found that the critical ratio (close to 1) of the fracture spacing to layer thickness is independent of the layer thickness (the dashed line shown in the same fig. 12). In addition, the fracture modeling approach also shows a 67 to 128 percent higher critical value of the fracture spacing to layer thickness ratio than that obtained from a stress analysis approach. Unfortunately, no published experimental data except those from numerical tests in the present paper are available on the observed differences in critical ratio of fracture spacing to layer thickness. We hope that our work will encourage more systematic studies, particularly experiments.

A difference of scale length of fracture spacing between fracture modeling approach and stress analysis approach is observed in our studies. As shown in figure 12, when we calculate the critical fracture spacing to layer thickness ratio, we found that the stress analysis approach predicts a linear relationship between critical fracture
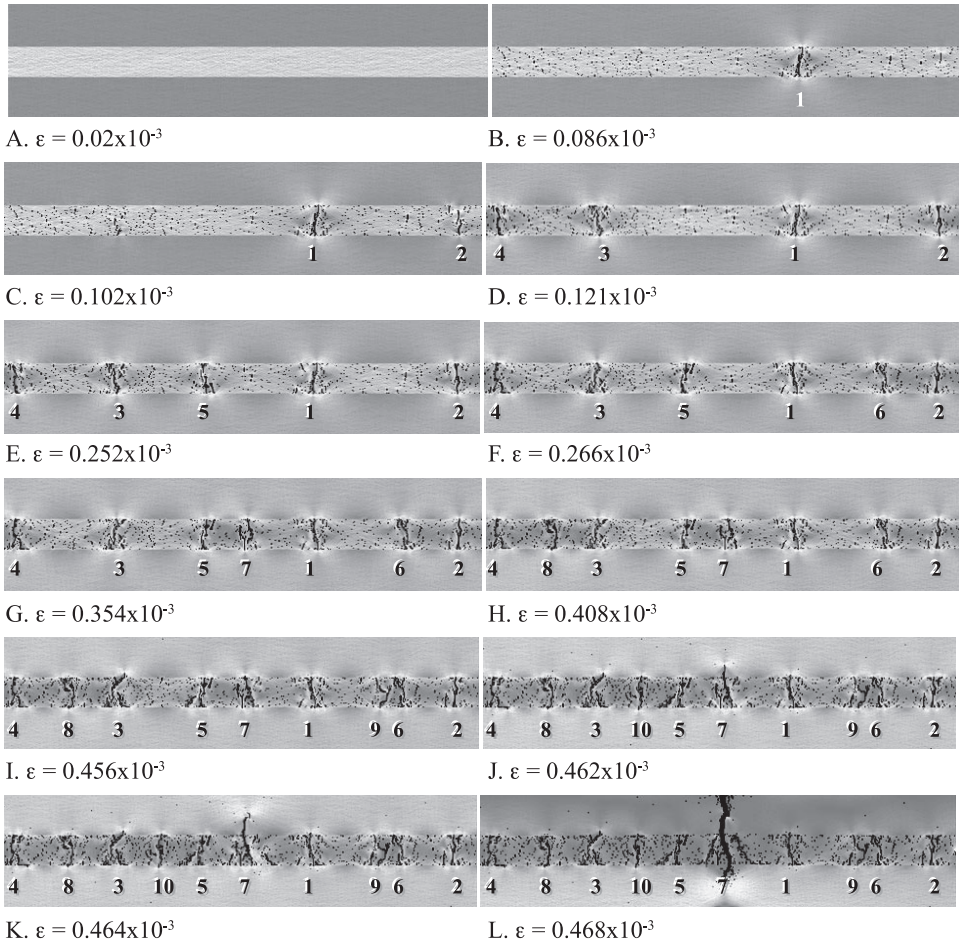
A. ε = 0.02x10⁻³

B. ε = 0.086x10⁻³

C. ε = 0.102x10⁻³

D. ε = 0.121x10⁻³

E. ε = 0.252x10⁻³

F. ε = 0.266x10⁻³

G. ε = 0.354x10⁻³

H. ε = 0.408x10⁻³

I. ε = 0.456x10⁻³

J. ε = 0.462x10⁻³

K. ε = 0.464x10⁻³

L. ε = 0.468x10⁻³

Fig. 8. Numerically obtained sequence of images of a portion of a crack pattern forming in a central layer (m=2, relatively heterogeneous) embedded between two neighboring layers. This sequence illustrates the "fracture infilling process and fracture saturation" described in the text. The numbers, 1-10, indicate the sequence of the fracture infilling. Note: the dark elements represent the nucleated flaw. Fractures form by connection of flaws. The shading intensity indicates the relative magnitude of the maximum shear stress within the elements. This figure shows how the evolution of fracturing in the model affects the stress distribution. The sequence of fracture formation is shown by the sequential notation on the figures.

spacing and layer thickness, whereas the fracture modeling approach reveals a non-linear relationship between critical fracture spacing and the layer thickness.

Effects of the Heterogeneity on Critical Fracture Spacing to Layer Thickness Ratio

In order to study the influence of heterogeneity on the fracture patterns and the critical fracture spacing to layer thickness ratio, we chose eight different values of the homogeneity index, *m*=1.1, 1.5, 2, 4, 6, 8, 10 and 15, for the central layer to setup models representing relatively heterogeneous to relatively homogeneous materials, while keeping other parameters constant. The mechanical properties and the model size are shown in table 1 for figure 13.

Figure 13 shows the eight models and the final stage of the modeling after the fractures are well-developed (that is, saturated). From our modeling we observed a
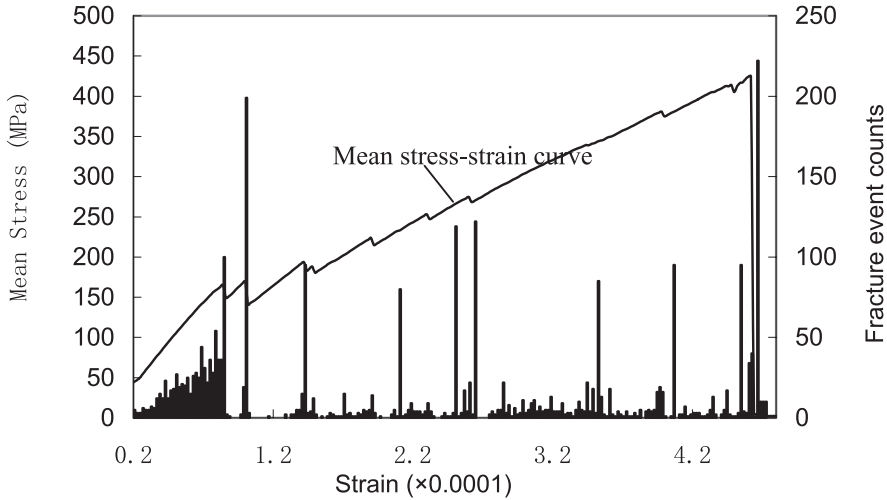
Fig. 9. Plots of numerically obtained mean stress (σ) and fracture event count (N) as a function of average strain (ε)

change in the way in which fracture occurred as the heterogeneity in the model was varied: for a relatively homogeneous model (as shown in figs. 13G and 13H), fracture formed through the propagation of newly nucleated small fractures in lines more or less perpendicular to the layer. For highly heterogeneous material model, however, it is found that fractures did not form by crack propagation, but rather formed by the coalescence of independent flaws (weaker elements).

Numerical results show that even a crack starts to propagate, it does not mean that it will propagate all the way to cut the thickness. In addition, the fracture nucleation sometimes starts from the interface, rather than from the interior of the layer, and the fracture propagation more or less takes a wavy path across the layer. As mentioned above, the theories mentioned by Hornig and others (1996) predict that cracks will tend to form in the middle of existing fractures of the layer, as that is ideally where the stress in the area will be largest, and the length scale of fracture spacing pattern decreases by a factor of 2 with each generation of fractures. In our models with heterogeneity considered, however, new fractures are observed to form at locations that are not always in the middle between the existing adjacent fractures.

Except for the influence of heterogeneity on fracture mode, numerical results also demonstrate that fracture event patterns are influenced greatly by the degree of heterogeneity of the materials. Figure 14 shows the cumulative fracture events as a function of loading step for various homogeneity indexes. The results show that the relatively heterogeneous models produce more fracture events than that of the relatively homogeneous model.

It is noted that the existence of plateau in each curve shown in figure 14 clearly indicates the reaching of fracture saturation.

The numerical results also show that although the patterns of fractures can be very complex, the length scale of fracture spacing shows an overall scaling behavior closely related to that in homogeneous materials. However, quantitatively, difference in length scale of fracture spacing is found between the heterogeneous and homogeneous models. Numerical simulations show that the critical fracture spacing to layer thickness ratio increases with increasing homogeneity index (representing heterogeneity's strength). By plotting the critical spacing to layer thickness ratio versus the
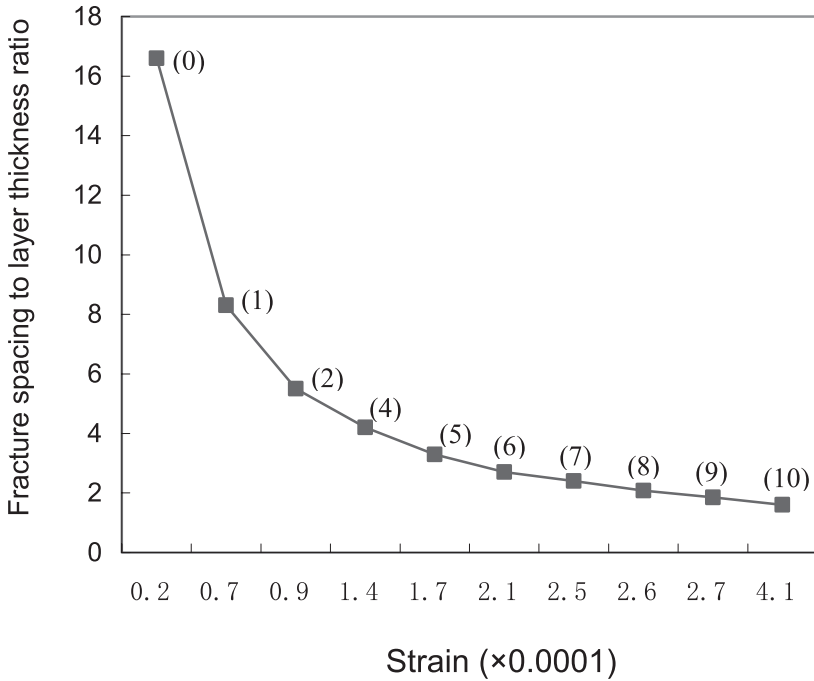
Fig. 10. Plot of the numerically obtained fracture spacing to layer thickness ratio (S/T_f) as a function of average strain (ε). (The number shown in the bracket is the number of fractures counted).

homogeneity index, *m*, we obtain the unique relation shown in figure 15. The critical spacing to layer thickness ratio is non-linearly related to the homogeneity index: a sharp change of the critical spacing to layer thickness ratio occurs in the range of $1 < m < 2$. As this index, *m*, goes to infinity (homogeneous), we observe a decrease in the curve slope and it can be predicated that the critical spacing to thickness ratio should asymptotically approach a constant value. This can be explained in terms of stress inhomogeneity or stress concentration. First, increasing heterogeneity of the layer increases the variation magnitude of the local stress concentrations, which results in more fractures forming in a lower loading stress level. Thus, increasing heterogeneity of the model will cause stress inhomogeneity or concentration and the critical fracture density will be reached at lower levels.

DISCUSSION

Numerical simulations have shed considerable light on fracture set development in layered model. In this section, we compare our fracture analysis approach with the former stress analysis approach, and discuss the implications of our fracture modeling results to the fracture pattern dynamics in layered materials.

Heterogeneity Effect

The initiation and propagation of fractures in the central rock layer causes a significant redistribution of the stresses surrounding the fractures. Correspondingly, the evolution of the fracture pattern and its interaction with the stress state is path dependent, and must be followed in the correct sequence if meaningful results are to be obtained. One of the important advantages of our modeling is that fractures are not pre-assigned to the layered models, but are allowed to evolve as the models are loaded

T_f=15

T_f=20

T_f=25

T_f=30

T_f=35   A. the numerical model   B. the numerically obtained minimum principal stress distribution
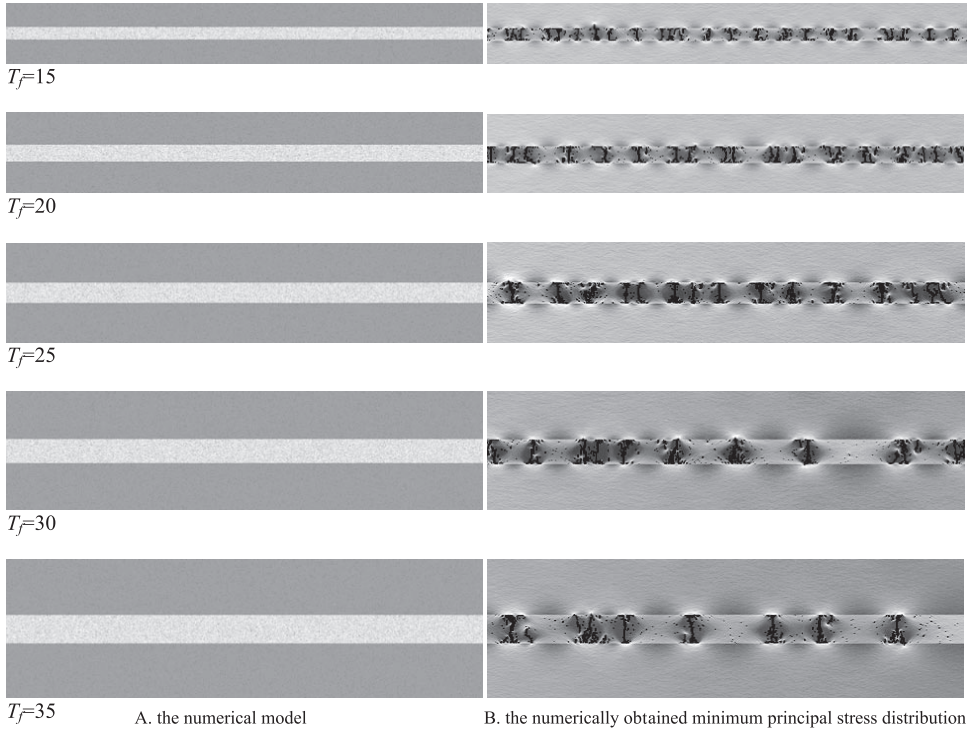
Fig. 11. Three layer models and the fracture spacing at saturation. The three layers with equal width, 600mm, have a central layer with height of T_f = 15, 20, 25, 30 and 35 mm, sandwiched between top and bottom layers with height of T_n = 30, 40, 50, 60 and 70 mm, respectively. Note: the dark elements represent the nucleated flaw. Fractures form by connection of flaws.

gradually. This will help us more clearly to understand the fracture spacing evolution and fracture saturation mechanisms.

As demonstrated in our modeling, opening-mode fractures form in response to tensile stress in the direction perpendicular to the fracture plane. The fracture formation process numerically obtained in this paper verifies that an opening-mode fracture cannot form between two fractures with a spacing to layer thickness ratio less than the critical value. There exists a critical ratio of fracture spacing to layer thickness that gives the lower limit for the fracture spacing to layer thickness ratio, that is the ratio at fracture saturation. Theories of fracture-pattern formation based on a static stress analysis approach (Bai and others, 2000) indicate that each generation of fractures should appear in the middle between the existing fractures, leading to successive halvings of the length scale of the pattern. This follows from the fact that ideally the stress between the existing fractures of the layer will be a maximum midway between two fractures. However, as shown in figures 8, 11 and 13, a near-perfect halving of existing fractures was seen only rarely in our numerical modeling. This is due to unevenness in the local stress distributions resulting from the existence of heterogeneity in the models.

The statistical description of failure phenomena in heterogeneous or disordered materials has drawn much attention in the past two decades; since then the understanding for the basic mechanisms leading to failure has grown and we have recognized the important role played by the material heterogeneities on the fracture patterns (for
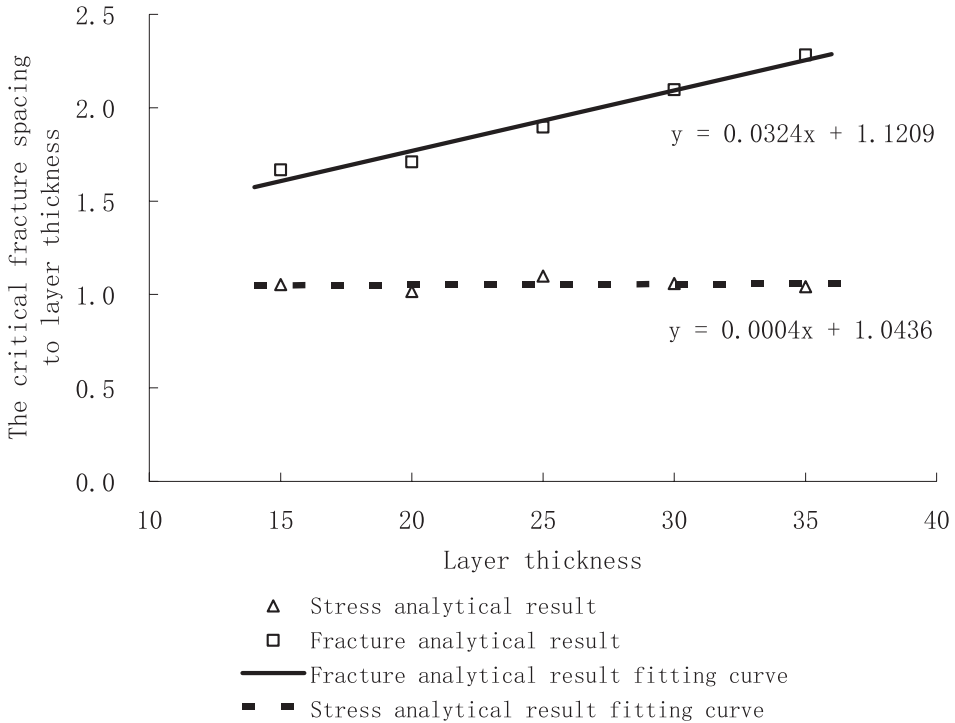
Fig. 12. Plot of the numerically obtained mean fracture spacing to layer thickness ratio (S/T_f) as a function of layer thickness (T_f) (each point showing the average value of four modeling results).

example, Horning and others, 1996). Our modeling shows clearly the dynamics of fracture pattern formation in models with heterogeneity considered. In the first stage of fracture pattern development, fractures nucleate at a small number of points or at a large number of points, depending on the degree of material heterogeneity of the models. In the case of a relatively homogeneous model, fractures propagate in fairly straight lines, usually in a direction sub-perpendicular to the layer interfaces. In runs with a relatively heterogeneous model, fractures tend to nucleate at the weaker points, and in many cases do not propagate long distances across the layer, but rather move in short steps from one weaker point to the next, occasionally meeting another fracture moving in a similar fashion.

Another regime of fracture patterns exists for a highly heterogeneous model, where fractures tend to have spacing that is very irregular and much less than the spacing in a homogeneous model. This spacing regime may be responsible for fracture swarms, such as discussed by Olson (2004). As shown in figure 15, although the numerically obtained length scale of the final fracture spacing is also proportional to the layer thickness, the constant of proportionality is found to be smaller for more heterogeneous models. With increasing heterogeneity, the stress in the layer will grow more nonuniformly and so there will be more opportunities for locations to reach the critical stress for fracture.

Effect of Delamination on the Critical Fracture Spacing to Layer Thickness Ratio

As shown in figures 11 and 13, another very commonly observed mode of fracture pattern formation is that fractures may nucleate and propagate along the interface
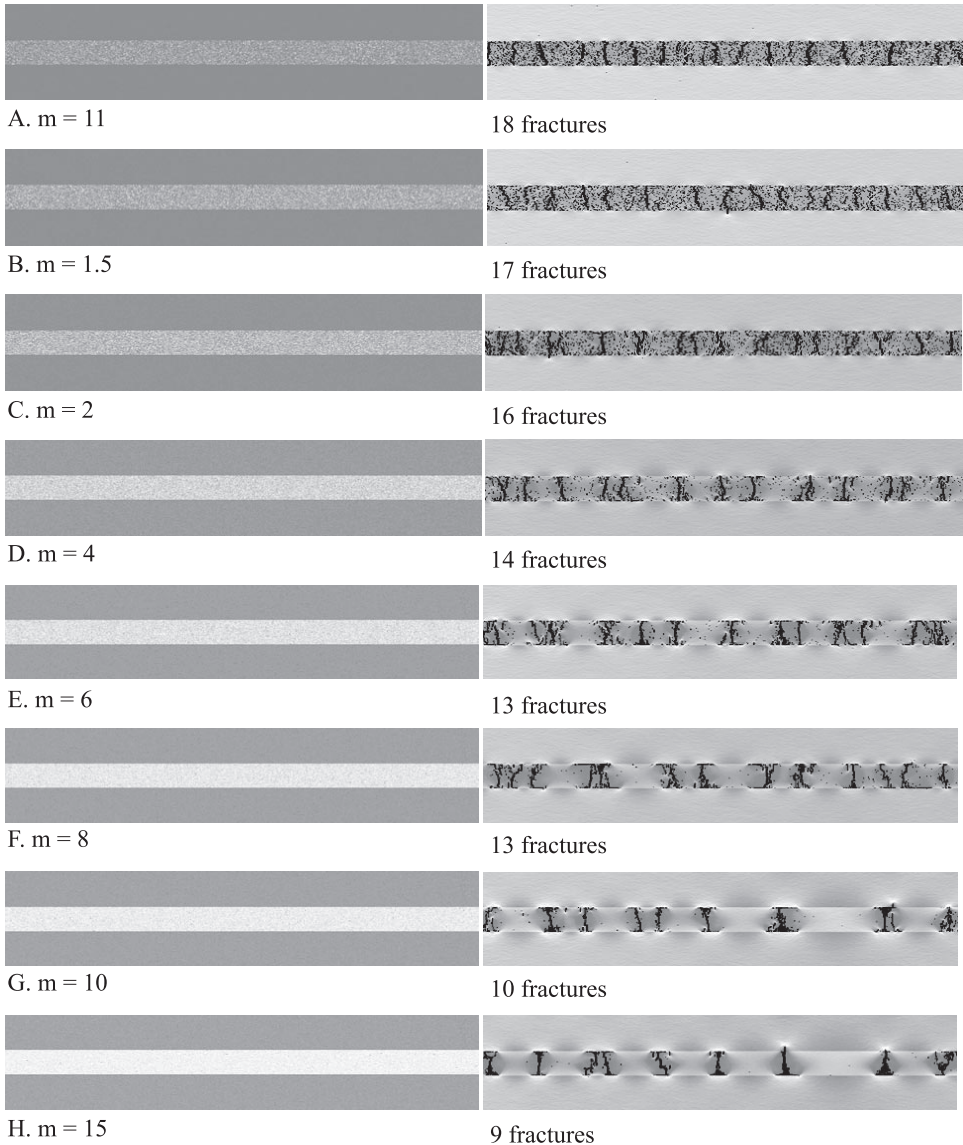
A. m = 11

18 fractures

B. m = 1.5

17 fractures

C. m = 2

16 fractures

D. m = 4

14 fractures

E. m = 6

13 fractures

F. m = 8

13 fractures

G. m = 10

10 fractures

H. m = 15

9 fractures

Fig. 13. Three layer models and the fracture spacing at saturation, with different homogeneity index, m=1.1, 1.5, 2, 4, 6, 8,10,15. The three layers with equal width, 600mm, have a central layer with height of $T_f = 30$mm, sandwiched between top and bottom layers with height of $T_n = 45$mm.

between layers, that is, delamination or decohesion (Hu and others, 1988; Drory and others, 1988). Physically, delamination will partially disconnect the fractured layer from the neighboring layers. In other words, once delamination begins the deformation in the fractured layer becomes less affected by the neighboring layers.

The mechanisms of delamination have been discussed by several authors such as He and Hutchinson (1989), Thouless (1989), and Cherepanov (1994), and Bai and others (2000) among others. Experimental results of Wu and Pollard (1995) show that delamination between the fracture layer and neighboring layers plays a significant role
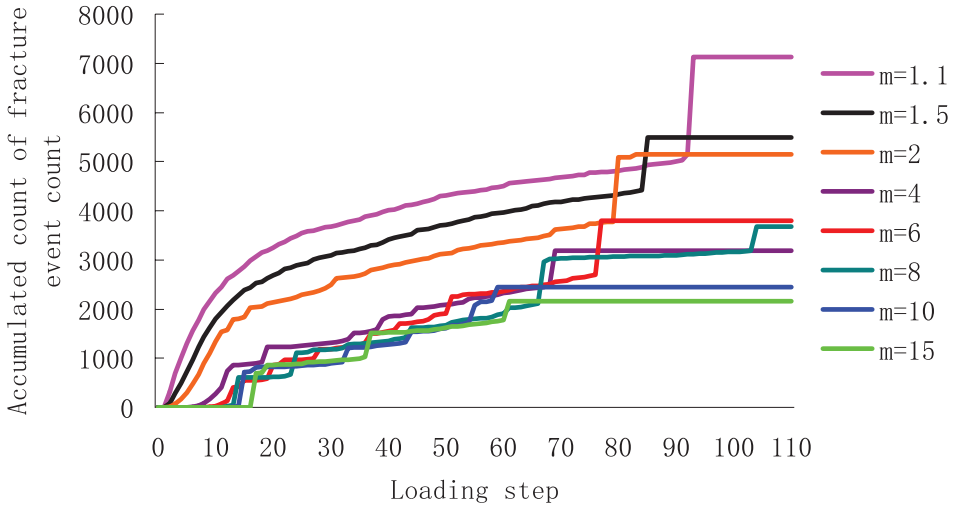
Fig. 14. Plots of the numerically obtained accumulated count of fracture events as a function of loading step for various homogeneity indices, showing the influence of heterogeneity on fracture patterns. (It is noted that the existence of plateau in each curve shown in figure 14 clearly indicates the reaching of fracture saturation.)

in affecting fracture behavior and leads to a larger spacing to layer thickness ratio than the ratio for completely bounded interface. Narr and Suppe (1991) and Wu and Pollard (1995) suggested that saturation is achieved at certain levels of strain when slip along layer interfaces and opening of pre-existing fracture replaces the development of new fractures as the dominant mechanism for strain accommodation. Bai and others (2000) numerically studied this delamination effect by postulating a model with
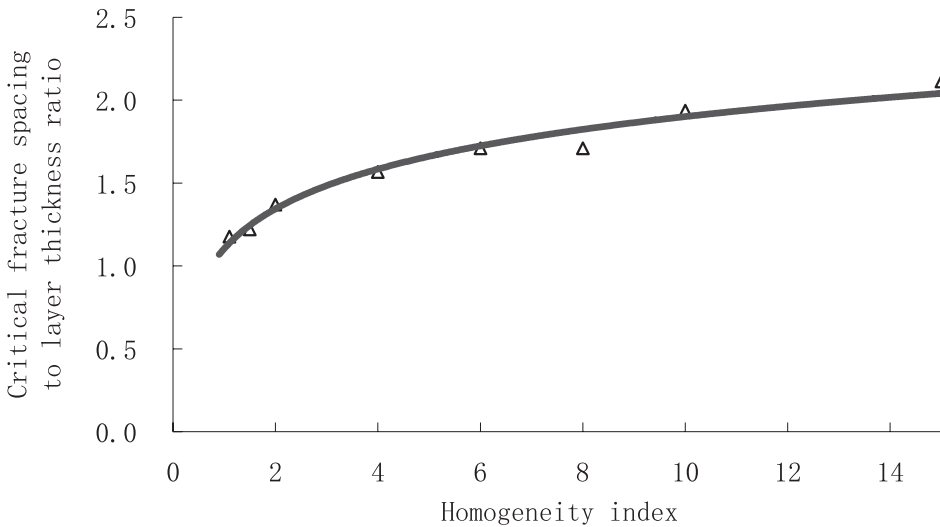

Fig. 15. Plots of the numerically obtained critical ratio of fracture spacing to layer thickness as a function of homogeneity index, showing the influence of heterogeneity on critical length scale (m=1.1, 1.5, 2, 4, 6, 8, 10 and 15).

a very soft thin layer between the fractured layer and the underlying layer. They used a static stress analysis approach to this problem and found that the critical fracture spacing to layer thickness ratio is about 9 to 10 times the value for the case of no delamination.

Our direct fracture modeling approach demonstrated how delamination would affect the fracture saturation behaviour and associated critical value of the spacing of fractures to the thickness of the fractured layer. During the fracture infilling process, the top and bottom layers apply a local traction at all points to the central embedded layer which has a nonzero shear modulus. Although the interface between layers is assumed to be perfectly bonded, numerical simulations show that the interface may not remain perfectly bounded at large strains and delamination may occur if the shear stress near the layer boundary is high enough. This delamination could change the local stress state significantly. One of the most important effects is that delamination will stop the transition of stress from the neighboring layers to the embedded central layer, and, in turn, prevent further infilling of fractures between existing fractures in the central layer. Consequently, this will result in a longer length scale of fracture spacing, and makes the critical spacing to layer thickness ratio much greater.

Effect of Throughgoing Fracture on the Critical Fracture Spacing to Layer Thickness Ratio

If the strength of the neighboring layer is not high enough, throughgoing fracture may occur. Although the increasing strain will result in sequential infilling that results in a decrease in fracture spacing, the subsequent development of throughgoing fracture precludes further fracture infilling, so that even larger increments of strain will not result in the formation of additional infilling fractures.

Generally, fractures in the confined layer terminate at the layer boundaries because the stress at the fracture tip drops below critical upon entering the layer boundaries. This occurs due to differences in mechanical properties such as Young's modulus or strength [refer to Watkins (ms, 1992) and Watkins and Green (1994) for analytical solutions]. In order for throughgoing fracture to grow, stress must remain critical as the fracture passes through neighboring layers of different mechanical properties. Thus, for a layer-confined fracture to grow into a throughgoing fracture, the fracture-normal tensile stress must increase to the tensile strength as the fracture passes into the neighboring layers. Under conditions of fracture-normal stretching as the driving mechanism, this can only be accomplished through an increase in extensional strain.

Once the fracture spacing is well-developed, however, less energy is required to extend an existing layer-confined fracture forming a throughgoing fracture cutting across the layer boundaries than to propagate a new fracture from a flaw within the layer between adjacent fractures.

It is worthy to mention that there are two types of fractures: (1) fractures may initiate at points (that is, a single failed element) and then grow upwards or downwards, one failed element at a time, or (2) they may coalesce from failed elements that are simply near one another. Our modeling shows that which type the fracture takes strongly depends on the heterogeneity of the material properties or the homogeneity index. Generally, a homogeneous material model will have more fractures of the first type, and a heterogeneous material model will have more fractures of the second type. In our simulation, as shown in figure 8, both fracture types are observed. As the central layer is relatively heterogeneous (m=2), most of the fractures demonstrate a second type fashion, that is, they coalesce from nearby failed elements. Whereas in the top and bottom layers, as the material is relatively homogeneous (m=6), we observed that a throughgoing fracture grows upwards and downwards, one failed element at a time.

It is found from the modeling that although the fractures in the central layer are formed by coalescence between isolated fractures, most of them are not shear mode fractures, they are opening mode fractures.

In this paper we performed numerical studies of fracture pattern formation in three layer models under quasistatical, slowly increasing strains; and reproduced many of the qualitative features seen in experiments and nature. We analyzed the pattern of fractures, and the dependence of the length scale on the strain. Generally, numerical simulations demonstrate that fracture spacing is inversely proportional to the magnitude of applied strain. As applied strain increases, the fracture spacing systematically decreases through the process of sequential infilling.

An important concept that we have numerically confirmed and quantified during these simulations is fracture saturation, which is attributed to stress relaxation caused by several reasons. The first way fracture may tend toward saturation levels requires a mechanism of strain accommodation: the fracture spacing initially decreases as extensional strain increases. At a certain ratio of fracture spacing to layer thickness, however, no new fractures form and the additional strain is accommodated by further opening of existing fractures. A second way fracture may tend toward saturation levels does not require a switch in strain accommodation mechanisms. As spacing between adjacent fractures decreases, overlapping stress reduction shadows dramatically reduce the effective fracture-normal tensile stress between the fractures, which when combined with the decrease in low strength flaws, requires extremely large additions of strain to cause further fracture infilling. Small regional variations in strain will not suffice to produce further infilling, and consequently the fractured layer can attain a "natural" state of fracture saturation without the need for opening along the pre-existing fractures. Such a situation predicts a higher critical ratio of fracture length scale. The third way fractures attain saturation relates to additional fractures, such as the interface delamination or the throughgoing opening-mode fracture that passes through the neighboring layers reaching their ultimate strength. All these fractures may prevent further infilling of new fractures, and may serve as another important mechanism to accommodate the applied strain.

We find that although the fracture spacing, as predicted theoretically by many other investigators using a static stress analysis approach, is proportional to layer thickness, the fracture modeling approach predicts a higher value of critical fracture spacing to layer thickness ratio. A comparison between stress analysis and fracture modeling of the three layer models reveals that the prediction of fracture spacing based on the stress state transition overestimates the fracture densities and predicted a lower value of critical fracture spacing to layer thickness ratio. Our numerical simulations demonstrate that fracture spacing at saturation increases as a function of layer thickness, but spacing is not linearly proportional to thickness. Instead, the fracture spacing to layer thickness ratio is found to be linearly proportional to the layer thickness. This observation may be considered as a theoretical explanation to fracture spacing data scatter observed in field or laboratory experiments.

The modeling results show that fracture patterns strongly depend on the heterogeneity of the model, that is, the distribution of mechanical properties in terms of the elastic constant and the breakdown strength. For weak disorder the fractures form through crack propagation, whereas for strong disorder the fractures form through the coalescence of initially independent smaller fractures nucleated from weak elements. The fracture distribution for heterogeneous model initially is sparser, and the final fracture pattern comprises many closely spaced short fractures. Another regime of fracture pattern exists for a highly heterogeneous model, where fractures tend to have spacing that is very irregular and much less than the spacing in a homogeneous model. This spacing regime may be responsible for fracture swarms, such as discussed by Olson (2004). Quantitatively, the critical value of fracture spacing to layer thickness ratio decreases as the disorder of the mechanical properties increases.

REFERENCES

Bai, T., and Pollard, D. D., 2000a, Fracture spacing in layered rocks: a new explanation based on the stress transition: Journal of Structural Geology, v. 22, p. 43–57.
—— 2000b, Closely spaced fractures in layered rocks: initiation mechanism and propagation kinematics: Journal of Structural Geology, v. 22, p. 1409–1425.
Bai, T., Pollard, D. D., and Gao, H., 2000. Explanation for fracture spacing in layered materials: Nature, v. 403, p. 753–756.
Bai, T., Maerten, L., Gross, M. R., and Aydin, A., 2002, Orthogonal Cross Joints: Do They Imply a Regional Stress Rotation: Journal of Structural Geology, v. 24, p. 77–88.
Becker, A., and Gross, M. R., 1996, Mechanism for joint saturation in mechanically layered rocks: an example from southern Israel: Tectonophysics, v. 257, p. 223–237.
Brady, B. H. G., and Brown, E. T., 1993, Rock Mechanics, second edition: London, Chapman and Hall, 98 p.
Cherepanov, G. P., 1994, On the theory of thermal stresses in a thin film on a ceramic substrate: Journal of Applied Physics, v. 75, p. 844–849.
Cobbold, P. R., 1979, Origin of periodicity: saturation or propagation: Journal of Structural Geology, v. 1, p. 96–97.
Cox, H. L., 1952, The elasticity and strength of paper and other fibrous materials: British Journal of Applied Physics, v. 3, p. 72–79.
Drory, M. D., Thouless, M. D., and Evans, A. G., 1988, On the decohesion of residually stressed thin films: Acta Metallurgica, v. 36, p. 2019–2028.
Fischer, M. P., Engelder, M. R., and Greenfield, R. J., 1995, Finite element analysis of the stress distribution around a pressurized crack in a layered elastic medium: implications for the spacing of fluid-driven joints in bedded sedimentary rock: Tectonophysics, v. 247, p. 49–64.
Garrett, K. W., and Bailey, J. E., 1977a, The effect of resin failure strain on the tensile properties of glass fibre-reinforced polyester cross-ply laminates: Journal of Materials Science, v. 12, p. 2189–2194.
—— 1977b, Multiple transverse fracture in 90^0 cross-ply laminates of a glass fibre-reinforced polyester: Journal of Materials Science, v. 12, p. 157–168.
Gross, M. R., 1993, The origin and spacing of cross joints: examples from Monterey Formation, Santa Barbara Coastline, California: Journal of Structural Geology, v. 15, p. 737–751.
Gross, M. R., and Engelder, T., 1995, Fracture strain in adjacent units of the Monterey Formation: Scale effects and evidence for uniform displacement boundary conditions: Journal of Structural Geology, v. 17, p. 1303–1318.
Gross, M. R., Fischer, M. P., Engelder, T., and Greenfield, R. J., 1995, Factors controlling joint spacing in interbedded sedimentary rocks: integrating numerical models with field observations from the Monterey Formation, USA, *in* Ameen, M. S., editor, Fractography: Fracture Topography as a Tool in Fracture Mechanics and Stress Analysis: London, Geological Society Special Publication, v. 92, p. 215–233.
He, M. Y., and Hutchinson, J. W., 1989, Kinking of a crack out of an interface: Journal of Applied Mechanics, v. 56, p. 270–278.
Helgeson, D. E., and Aydin, A., 1991, Characteristics of joint propagation across layer interfaces in sedimentary rocks: Journal of Structural Geology, v. 13, p. 897–911.
Hobbs, D. W., 1967, The formation of tension joints in sedimentary rocks: an explanation: Geological Magazine, v. 104, p. 550–556.
Hornig, T., Sokolov, I. M., and Blumen, A., 1996, Patterns and scaling in surface fragmentation processes: Physical Review E, v. 54(4), p. 4293–4298.
Hu, M. S., Thouless, M. D., and Evans, A. G., 1988, Decohesion of thin films from brittle substrates: Acta Metallurgica, v. 36, p. 1301–1307.
Huang, Q., and Angelier, J., 1989, Fracture spacing and its relation to bed thickness: Geological Magazine, v. 126, p. 355–362.
Ji, S., and Saruwatari, K., 1998, A revised model for the relationship between joint spacing and layer thickness: Journal of Structural Geology, v. 20(11), p. 1495–1508.
McQuillan, H., 1973, Small-scale fracture density in Asmari Formation of southwest Iron and its relation to bed thickness and structural setting: American Association of Petroleum Geologists Bulletin, v. 57, p. 2367–2385.
Narr, W., and Lerche, I., 1984, A method for estimating subsurface fracture density in core: American Association of Petroleum Geologists Bulletin, v. 66, p. 637–648.
Narr, W., and Suppe, J., 1991, Joint spacing in sedimentary rocks: Journal of Structural Geology, v. 13, p. 1037–1048.
Olson, J. E., 2004, Predicting fracture swarms – the influence of subcritical crack growth and the crack-tip process zone on joint spacing in rock, *in* Cosgrove, J. W., and Engelder, T., editors, The Initiation, Propagation, and Arrest of Joints and Other Fractures: London, Geological Society Special Publication, v. 231, p. 73–87.
Parvizi, A., and Bailey, J. E., 1978, On multiple transverse cracking in glass fibre epoxy cross-ply laminate: Journal of Materials Science, v. 13, p. 2131–2136.

Pollard, D. D., and Segall, P., 1987, Theoretical displacements and stresses near fractures in rocks: with applications to faults, joints, veins, dikes and solution surfaces, *in* Atkinson, B. K., editor, Fracture Mechanics of Rock: London, Academic Press, p. 277–349.

Price, N. J., 1966, Fault and Joint Development in Brittle and Semi-Brittle Rocks: Oxford, Pergamon Press, 176 p.

RFPA User Manual, 2005: Dalian Mechsoft Co., Ltd., 4 p.

Rives, T., Razack, M., Petti, J. P., and Rawnsley, K. D., 1992, Joint spacing: analogue and numerical simulations: Journal of Structural Geology, v. 14, p. 925–937.

Spyropoulos, C., Scholz, C. H., and Shaw, B. E., 2002, Transition regimes for growing crack populations: Physical Review E, 65 056105-1-10.

Tang, C. A., 1997, Numerical simulation of progressive rock failure and associated seismicity: International Journal of Rock Mechanics and Mining Sciences, v. 34, p. 249–261.

Thouless, M. D., 1989, Some mechanics for the adhesion of thin films: Thin Solid Films**,** v. 181, p. 397–406.

Watkins, T. R., ms, 1992, The fracture behaviour of silicon carbide-graphite composites: Pennsylvania State University, Ph. D. Thesis, p. 287.

Watkins, T. R., and Green, D. J., 1994, Fracture behaviour of CVD SiC-coated graphite: II. Conditions for the onset of multiple cracking: Journal of the American Ceramic Society, v. 77, p. 717–720.

Wu, H., and Pollard, D. D., 1991, Fracture spacing, density, and distribution in layered rock masses: results from a new experimental technique, *in* Roegiers, J. C., editor, Rock Mechanics as a Multidisciplinary Science: Rotterdam, Balkema, Proceedings of the 32nd U. S. Symposium on Rock Mechanics, p. 1175–1184.

———— 1992, Propagation of a set of opening-mode fractures in layered brittle materials under uniaxial strain cycling: Journal of Geophysical Research, v. 97, p. 3381–3396.

———— 1993, Effect of strain rate on a set of fractures: International Journal of Rock Mechanics and Mining Science and Geomechanics Abstracts 30, p. 869–872.

———— 1995, An experimental study of the relationship between joint spacing and layer thickness: Journal of Structural Geology, v. 17, p. 887–905.